energy&fuels

Article

Cite This: Energy Fuels 2019, 33, 6038−6047

pubs.acs.org/EF

# Evaluating the Transport Behavior of $CO_2$ Foam in the Presence of Crude Oil under High-Temperature and High-Salinity Conditions for Carbonate Reservoirs

Guoqing Jian,[†] Leilei Zhang,[†] Chang Da,[‡] Maura Puerto,[†] Keith P. Johnston,[‡] Sibani L. Biswal,*[,†] and George J. Hirasaki*[,†]

[†]Department of Chemical and Biomolecular Engineering, Rice University, Houston, Texas 77005, United States

[‡]McKetta Department of Chemical Engineering, The University of Texas at Austin, Austin, Texas 78712, United States

Supporting Information

**ABSTRACT:** An amine-based surfactant, Duomeen TTM, was evaluated for foam flooding in carbonate rock at high temperature (120 °C), high salinity (22% total dissolved solids), and $CO_2$−oil miscible conditions. We demonstrate enhanced oil recovery by utilizing $CO_2$ foam under miscible conditions in the presence of crude oil. The foam was generated in situ by both co-injection and surfactant alternating gas injection modes. Foam transport and propagation were characterized as a function of the foam quality, shear rate, permeability, surfactant concentration, and method of injection. Finally, we utilize the experimental results to obtain the parameters for the STARS foam model by optimizing multiple variables related to the dry out, shear thinning, and surfactant concentration effects on foam transport. Enhanced oil recovery utilizing $CO_2$ foam under miscible conditions in the presence of SMY crude oil was able to decrease oil saturation to 3.0%. It was also determined that significantly more injected pore volumes were required for the foam to reach the steady state in the presence of SMY crude oil. A foam simulation process in a heterogeneous reservoir is conducted applying the parameters obtained. The TTM $CO_2$ foam generated significantly reduces the mobility of $CO_2$ in the high permeability layers, which results in an improved swept volume in the low permeability zone that significantly improves oil recovery when epoil = 1 and fmoil = 0.5. Oil saturation parameters play important roles in the effectiveness of $CO_2$ foam: large epoil and small fmoil will reduce the efficiency for TTM $CO_2$ foam.

## 1. INTRODUCTION

Carbon dioxide ($CO_2$) flooding[1] has been widely tested in the past 40 years, and its displacement efficiency[2−5] is high when the pressure is higher than the minimum miscible pressure of $CO_2$ for the oil in question. The low viscosity and low density of $CO_2$ cause viscous fingering and gas override. In addition, the reservoir heterogeneity favors $CO_2$ transport through the high permeability layer. These three characteristics lead to an early gas breakthrough and thus lower the sweep efficiency of $CO_2$ gas flooding.

$CO_2$ foam[6−16] can increase the apparent viscosity of $CO_2$ by decreasing the relative permeability of $CO_2$ gas in porous media. Thus, the mobility of $CO_2$ can be decreased, making $CO_2$ foam a promising technique for enhancing the oil recovery of miscible $CO_2$ flooding process. The success of a $CO_2$ foam flooding relies on the choice of the surfactant for a specific reservoir, understanding the transport phenomenon of $CO_2$ foam in porous media,[17] and its oil recovery mechanism under miscible conditions.

The surfactants used in $CO_2$ foam processes could be anionic,[18] cationic,[19] zwitterionic,[20] and nonionic surfactant.[21,22] Anionic surfactants are promising candidates for $CO_2$ foam enhanced oil recovery (EOR) in sandstone reservoirs because of their low adsorption[23] on the negatively charged formation. Cationic[24] and nonionic[25] surfactants are typically used for carbonate formations to minimize surfactant adsorption via electrostatic interactions. Switchable nonionic to cationic ethoxylated amine surfactants[26] are promising for high-temperature high-salinity carbonate reservoirs, because they can be protonated by carbonic acid formed when high-pressure $CO_2$ is dissolved in brines under reservoir conditions. Zwitterionic surfactants, depending on their specific molecular structure, are promising for their application in both sandstone and carbonate reservoirs if proven to have low adsorption on the formation surfaces. The uncertainty of transport phenomenon of $CO_2$ foam in porous media includes a minimum pressure gradient of generating foam,[17] the foam rheology sensitivity to permeability,[27] and different injection strategies.[28,29] Understanding the oil recovery mechanisms of miscible $CO_2$ foam is required to better apply $CO_2$ foam for EOR.

Furthermore, research regarding how $CO_2$ foam is transported in core systems in the presence of crude oil and its related modeling and simulation studies is limited. Here, we investigate $CO_2$ foam under high temperature and high salinity conditions for carbonate reservoirs in the presence of SMY crude oil. Duomeen TTM, a cationic diamine surfactant, was utilized to generate $CO_2$ foam. This surfactant has been previously reported to generate strong $CO_2$ foam under high temperature (120 °C) and high salinity conditions in bead pack systems[30,31] without the limitation of a minimum pressure gradient under a high fractional gas flow. In this study, $CO_2$

Received: March 5, 2019
Revised: May 8, 2019
Published: June 20, 2019






DOI: 10.1021/acs.energyfuels.9b00667
Energy Fuels 2019, 33, 6038−6047

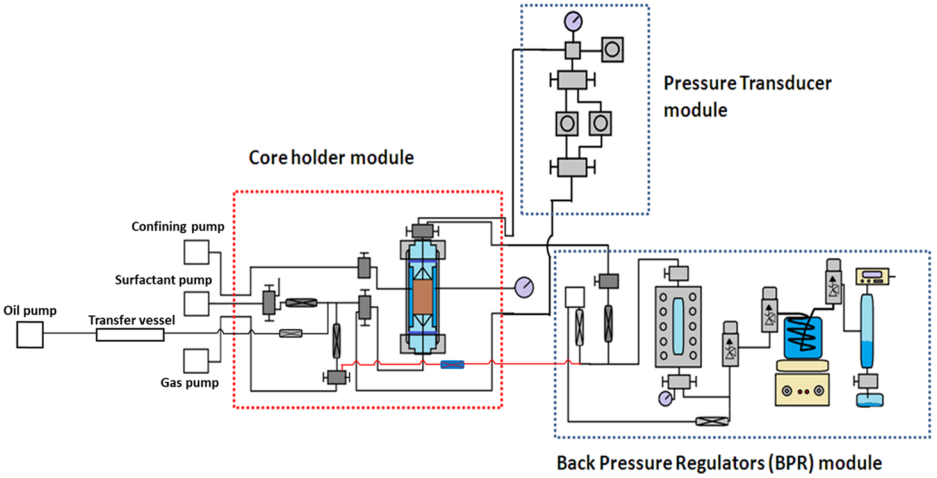


**Figure 1.** Schematic of high-temperature and high-pressure experimental testing system for $CO_2$ foam flooding.

foam rheology in limestone cores is characterized, and the foam parameters were obtained based on the STARS foam model.[32,33] A sensitivity analysis of the oil saturation foam parameters was performed and determined that TTM foam has good mobility control for large values of fmoil and small values of epoil. These results highlight the importance of studying the oil−foam interactions in porous media.

## 2. MATERIALS AND METHODS

**2.1. Materials.** Sodium chloride (NaCl, certified ACS, Sigma-Aldrich), calcium chloride dihydrate ($CaCl_2{\cdot}2H_2O$, certified GR ACS grade, EMD Chemicals), magnesium chloride hexahydrate ($MgCl_2{\cdot}6H_2O$ certified GR ACS grade, EMD Chemicals) are used for the brine and used as received. Duomeen TTM, a cationic diamine surfactant ($C_{16\text{-}18}N(CH_3)C_3N(CH_3)_2$ (TTM), AkzoNobel) was utilized to generate foam. This surfactant has been previously reported to generate strong $CO_2$ foam under high temperature (120 °C) and high salinity conditions (22% total dissolved solids[30]) and used as received. The surfactant solutions tested in the experiments were formed by dissolving the surfactant into a 22% total dissolved solids (TDS) brine (182.31 g/L NaCl, 77.25 g/L $CaCl_2{\cdot}2H_2O$, 25.62 g/L $MgCl_2{\cdot}6H_2O$) after protonation with HCl to achieve surfactant solutions that vary from 0.05 to 1 wt %.

**2.2. Experimental Setup for $CO_2$ and $CO_2$ Foam Experiments.** The setup for core flooding[17] contains pump systems and three modules (core holder module, pressure transducer module, and back pressure regulators (BPRs) module), as shown in Figure 1. The details of pumps system and three modules are shown in Supporting Information from Figures S1 to S3.

The pump system contains an auxiliary pump, which provides a confining pressure to the core in the core holder. Other pumps (ISCO Teledyne 260D pumps) deliver fluids including surfactant solution, crude oil(through a transfer vessel), and $CO_2$ into the core. The core holder module consists of a high-pressure core holder made with stainless steel and two end pieces made with Hastelloy. Different transducers with various ranges were used to record the pressure drop across the core and the system pressure during the core flooding experiments.

The back pressure regulator (BPR) system consists of three relief valves and an auxiliary HPLC pump. The first relief valve is set at 3400 psi, the second is between 2500 and 3000 psi, and the third is at 1200 psi. Because a constant enthalpy pressure drop results in a temperature drop of $CO_2$, the flow line between the 2500 and 1200 psi relief valves is immersed in a hot water bath to ensure that the temperature remains above 0 °C for preventing freezing of the effluent. Distilled water is injected through relief valves by an auxiliary pump for keeping the relief values always open at the set pressure; this maintains the back pressure stable mitigating wild pressure oscillations.

**2.3. Procedure of $CO_2$ and $CO_2$ Foam Flooding.** *2.3.1. Core Vacuuming and Water Saturation.* The water saturation before core flooding includes the following steps: the core is (1) wrapped with a two-layer shrink Teflon film with an aluminum foil in the middle (as shown in Figure S4) and then inserted in a rubber sleeve and mounted in the core holder where confining pressure of 600−900 psi is applied to the core (2) vacuumed by vacuum pump (Welch 1400B-01) until reading in vacuum gauge is < −29 inHg (3) saturated with brine to determine pore volume based on the brine imbibed from the burette connected to the set up; dead volumes of tubing and valves are previously determined.

*2.3.2. Water Phase Permeability.* The permeability of the core was determined at room temperature by flowing diluted brine (1/10 of the original ionic strength of the 22% TDS brine) at different flow rates to obtain the pressure drop across the core. The viscosity at room temperature of the 1/10 brine is approximately 1 cp. The flow rate as superficial velocity is plotted against pressure drop to obtain the slope as shown in eq 1 to calculate the permeability.

$$k = \frac{Q \times \mu \times L}{A \times (P_{in} - P_{out})} \quad (1)$$

where $k$ is the absolute permeability of the core, $Q$ is the volumetric flux, $\mu$ is the dynamic viscosity of 1/10 ionic strength of 22% TDS brine, $L$ is the length of the core, $A$ is the cross-sectional area of the core, and $P_{in} - P_{out}$ is the pressure drop across the core.

*2.3.3. Core Flooding Experiments with $CO_2$ and $CO_2$ Foam.* Core flooding experiments were performed using Indiana limestone cores (Kocurek Industries Inc.). The majority of the Indiana limestone is $CaCO_3$ with some dolomite ($CaMg(CO_3)_2$), silica, and clays, as previously measured using energy dispersive X-ray (EDX, FEI Quanta 400 ESEM FEG) spectroscopy.[34] $CO_2$ foam experiments were initially performed in the absence of crude oil to evaluate in situ foam generation. Both co-injection or surfactant-alternating-gas (SAG) injection modes were utilized for $CO_2$ foam generation experiments.

Experiments with SMY crude oil for EOR were performed using a two-phase saturated carbonate core. This crude oil is previously reported to have an API gravity of 30.3° and asphaltene content of 1.86%.[35] The core was first vacuum evacuated and then saturated with 22% TDS brine at ambient conditions. This brine was then displaced with SMY crude oil. Subsequently, a brine flood at 4 ft/day was conducted leaving the core with two-phase saturation of brine and residual oil. After the brine flood, the pressure and temperature of the system were increased to 3400 psi and 120 °C, respectively. $CO_2$ flooding was conducted after brine flood for about 4 pore volumes (PV). Co-injection of $CO_2$ and brine was followed after the $CO_2$ flood. The $CO_2$ and brine flood was conducted at 4 ft/day with gas


DOI: 10.1021/acs.energyfuels.9b00667
Energy Fuels 2019, 33, 6038−6047

fraction flow at 80%. Foam flooding was conducted after $CO_2$ and brine flood for about 10 PV until the foam reaches a steady-state apparent viscosity. Steady-state foam experiments in the presence of residual oil or with some fractional flow of oil were conducted afterward.

**2.4. STARS Foam Modeling and Parameter Estimation.** The STARS foam model[32,33,36,37] is widely used to simulate foam flow in porous media. This foam model assumes that the foam flow is at the local equilibrium condition. In the STARS model, the gas relative permeability, $k_{rg}^{f}$, in the presence of the foam was modified with the mobility reduction factor FM by multiplying the gas relative permeability without foam $k_{rg}^{nf}$, as described in eq 2.

$$k_{rg}^{f} = k_{rg}^{nf} \times \mathrm{FM} \tag{2}$$

where $k_{rg}^{f}$ is the gas relative permeability in the presence of the foam, $k_{rg}^{nf}$ is the gas relative permeability in the absence of the foam.

$$\mathrm{FM} = \frac{1}{1 + \mathrm{fmmob} \times F_{water} \times F_{surf} \times F_{shear} \times F_{oil} \times \ldots} \tag{3}$$

In the FM function shown in eq 3, fmmob is a base foam mobility reduction term without the influences of different factors. The different factors governing the FM are summarized by eqs 4–7

$$F_{water} = 0.5 + \frac{\arctan[\mathrm{epdry}(S_w - \mathrm{fmdry})]}{\pi} \tag{4}$$

$$F_{surf} = \begin{cases} \left(\dfrac{C_{sw}}{\mathrm{fmsurf}}\right)^{\mathrm{epsurf}} & \text{for } C_{sw} < \mathrm{fmsurf} \\ 1 & \text{for } C_{sw} \geq \mathrm{fmsurf} \end{cases} \tag{5}$$

$$F_{shear} = \left(\frac{\mathrm{fmcap}}{N_{Ca}}\right)^{\mathrm{epcap}} \tag{6}$$

$$F_{oil} = \begin{cases} 0 & \text{for } S_o > \mathrm{fmoil} \\ \left(\dfrac{\mathrm{fmoil} - S_o}{\mathrm{fmoil} - \mathrm{floil}}\right)^{\mathrm{epoil}} & \text{for floil} < S_o < \mathrm{fmoil} \\ 1 & \text{for } S_o < \mathrm{floil} \end{cases} \tag{7}$$

In the *F*-functions, the ep values describe the sharpness or of how fast the *F* functions change, and the fm value in each function represents the critical value. Specifically, fmdry is the limiting water saturation, fmcap is the reference capillary number, $N_{Ca}$ is the capillary number, fmsurf is the critical surfactant concentration when foam strength starts to decay as surfactant concentration decreases, fmoil is the critical oil saturation where foam completely collapses, and floil is the lower limit of oil saturation, below which foam strength is not affected.

In this study, the effect of the gas fraction, injection rate, and surfactant concentration was studied. The parameters of the three functions were obtained using a linear regression[37] analysis and summarized in the Supporting Information from eqs S1 to S15. The oil-dependent function will be further discussed in the foam simulation results.

**2.5. Foam Simulation Using Estimated STARS Foam Parameters.** The foam simulation was performed using the CMG-STARS with the parameters that were obtained from the experimental data of TTM $CO_2$ foam in the core. The parameters used including dry-out effect, shear thinning effect, and surfactant concentration effect. All of these parameters can be obtained from the two-phase flow (gas/surfactant) steady-state experiments. For the oil saturation-dependent function, a sensitivity analysis was performed in the reservoir model using different oil saturation-dependent function parameters including fmoil and epoil. The oil saturation or $CO_2$ saturation using different oil saturation-dependent function parameters was analyzed and discussed.

## 3. RESULTS AND DISCUSSION

**3.1. Experiments and Modeling of TTM $CO_2$ Foam in the Absence of Crude Oil.** *3.1.1. Foam in Situ Generation Test by Co-injection.* The foam flooding experiments were conducted in 321 mD Indiana limestone core, 120 °C, 3400 psi at 4 ft/day with high-quality fractional gas flow, fg = 0.8. Previously, it was reported that a minimum pressure gradient (MPG) was needed at 4 ft/day and fg = 0.8 for the switchable surfactant Ethomeen C12 to generate $CO_2$ foam under the same experimental temperature and pressure conditions described here.[17] The MPG can be a serious issue, especially when the gas and surfactant are transported deep into the reservoir, where the local pressure gradient may not be large enough to generate foam.

$CO_2$ foam generation in the limestone core was typically divided into three periods. The first period corresponds to surfactant and gas mixing interval (0–0.3 pore volumes (PV)). The second period was foam generating in situ (0.3–1 PV). The third after 1 PV injection, the foam has been fully developed under test conditions. After that another 3 PV of surfactant and gas was continued to be co-injected into the core, which maintains the foam at the steady state. For the in situ foam generation tests in the Indiana limestone core, the mixing zone is about 0.3 PV (0.3 × 6 in. = 1.8 in. = 4.6 cm). As shown in Figure 2 for the TTM surfactant-stabilized $CO_2$ foam, the MPG was negligible when the fractional gas flow was as high as 0.8. This represents a large disjoining pressure whereby the liquid lamella films stabilized by TTM surfactant with the $CO_2$ as the external phase can sustain high capillary pressures.

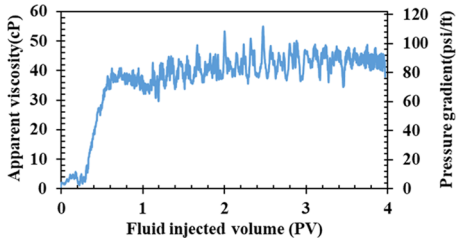


**Figure 2.** In situ foam generation of 1% TTM (pH = 7) foam in an Indiana limestone core ($k$ = 321 mD, 4 ft/day, fg = 0.8, $L \times D$ = 6 × 1.5 in., 120 °C, 3400 psi).

As an MPG was not a concern, the local equilibrium assumption of the STARS foam model could be satisfied. This condition means that in each grid block of the foam simulation process where gas and water phases are present with the transport of surfactant species, a local foam can be generated. Thus, the relative permeability of the gas phase can be described by the different *F*-functions in the STARS model. In the following experiment, the foam parameters in the dry-out function, shear thinning function, and surfactant concentration function were obtained by fitting to the experimental data. The relative permeability data and curve could be found in Table S1 and Figure S5 in the Supporting Information.

Additionally, the permeability of the core was measured before and after each experiment by flushing the core with brine from the inlet to outlet. It was assumed that when the permeability reaches to more than 95% of the original value, the core is restored, and the foam data can be used for foam modeling and parameters fitting process.



DOI: 10.1021/acs.energyfuels.9b00667
Energy Fuels 2019, 33, 6038–6047

*3.1.2. Effect of Injection Mode on TTM $CO_2$ Foam Generation.* For field applications, the SAG injection mode is oftentimes used to ameliorate potential injectivity issues. To compare injection strategies, both co-injection and SAG modes were utilized to investigate in situ $CO_2$ foam generation, as shown in Figure 3. In the SAG method, we inject a 0.5 PV cycle with a 20% surfactant slug (0.1 PV) followed by an 80% $CO_2$ gas slug (0.4 PV). Note that it requires more total pore volumes in the SAG mode compared to the co-injection mode for the $CO_2$ foam to reach the steady state. In situ $CO_2$ foam generation was observed in the first PV injection for both methods, and the maximum $CO_2$ foam strength with SAG after 2 PV was very close to the co-injection method.

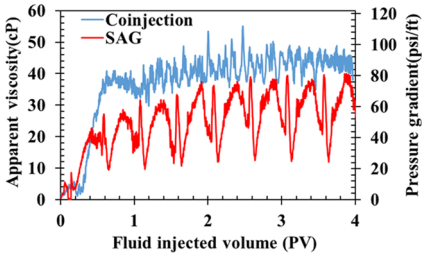


**Figure 3.** Comparison between co-injection and surfactant alternating gas (SAG) injection methods using 1% TTM solution for in situ foam generation in Indiana limestone ($k$ = 321 mD, 4 ft/day, fg = 0.8, $L \times D$ = 6 × 1.5 in., 120 °C, 3400 psi). Each 0.5 PV injection cycle for SAG is 0.1 PV surfactant solution followed by 0.4 PV $CO_2$.

*3.1.3. Effect of Permeability on the Foam Quality Scan and Dry-Out Function Parameters.* The foam quality is defined as the volumetric fractional flow rate of the gas phase relative to the total flow rate. The foam quality scans can be conducted by changing the fractional flow ratios of the gas and aqueous phases, which will result in different foam apparent viscosities at different foam qualities, as shown in Figure 4. To evaluate the influence of the core permeability on $CO_2$ foam quality, two different cores materials are studied. The results shown in Figure 4 illustrate how the foam apparent viscosity increases when the core permeability increases from 54 to 321 mD[38,39] The pressure gradient in the high and low permeability cores varied between 10−80 and 50−320 psi/ft and between 10 and 90% foam qualities, respectively. These test results indicate that the $CO_2$ foam has good injectivity in carbonate formation with the permeability in the hundreds mD. However, injectivity may be an issue in cores with tighter permeabilities (<100 mD).

The foam quality scan data was then fitted by the foam dry out function to estimate the fmmob, epdry, and fmdry values, which is then used for the foam simulation. The fitting curve based on the STARS foam model is shown by the continuous curve shown in Figure 4. Moreover, for the foam in 321 mD core, the foam can maintain a high value of apparent viscosity of nearly 38 cP when the fractional gas flow (foam quality) equals 95%. At high foam qualities, the saturation of the gas phase is high, and thus the capillary pressure is high. This indicates that the TTM surfactant-stabilized lamella films within the $CO_2$ foam are able to withstand large capillary pressures, which explains the stability of TTM $CO_2$ foams. In the 54 mD core, note that the $CO_2$ foam strength decreases for foam qualities above 80%. This earlier transition quality (fg = 80%) in 54 mD compared to that (fg = 95%) in the 321 mD core can be explained by the fact that at lower permeabilities, the average pore radius is much smaller. Since the capillary pressure is inversely proportional to the capillary radius, the capillary pressure is much higher. Thus, the $CO_2$ foam lamella becomes less stable at lower permeabilities due to the higher capillary pressure at a given foam quality.

*3.1.4. Effect of the Surfactant Concentration on the Foam Strength.* The surfactant concentration is another important parameter that influences the foam strength and foam transport behavior in porous media. This is particularly true in the reservoir where surfactant dispersion and adsorption occur. Therefore, it is important to understand the role of the surfactant concentration on foam transport and obtain the corresponding concentration-dependent function parameters. To evaluate the role of the surfactant concentration,[40] various surfactant solutions ranging from 0.05 to 1.0 wt %, were used for $CO_2$ foam experiments in the 321 mD core. The experiments were performed at a fixed 80% foam quality and superficial velocity of 4 ft/day. After each foam test, the core was restored by flushing with 22% TDS brine until the permeability measured was close to the original value (within 5%) and no surfactant produced from the effluent.

In general, it takes more time for the foam to reach the steady state at lower surfactant concentrations, as shown in Figure 5a. For surfactant concentrations above 0.25%, $CO_2$ foam can reach a steady-state foam strength within 1 PV, whereas for surfactant concentrations below 0.1%, 2−4 PV is required to reach the steady state. It is important to note that at different surfactant concentrations, the apparent viscosity of the steady-state foam varies. To determine the surfactant-related function parameter for the STARS foam model, a multivariable optimization fitting is performed. The critical

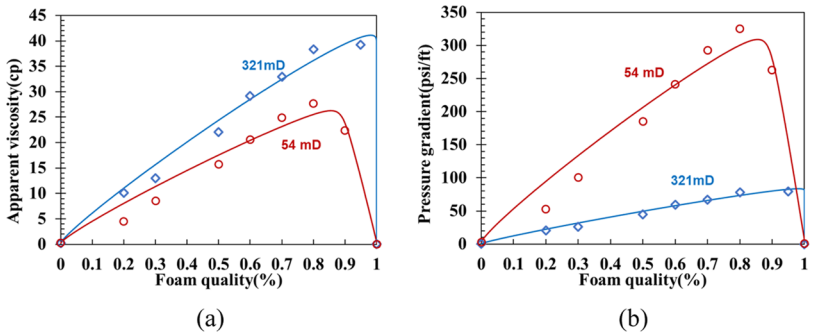


**Figure 4.** Effect of the permeability on the foam quality via (a) apparent viscosity and (b) pressure gradient, using 1% TTM foam with a 321 mD (blue) and 54 mD (red) core sample.



DOI: 10.1021/acs.energyfuels.9b00667
Energy Fuels 2019, 33, 6038−6047

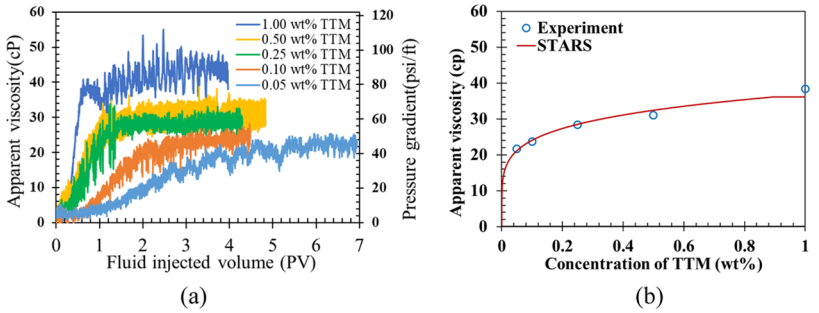


**Figure 5.** (a) Effect of the surfactant concentration on $CO_2$ foam generation in Indiana limestone ($k$ = 321mD, 4 ft/day, fg = 0.8, 120 °C, 3400 psi) and (b) the STARS model fit of the steady-state foam strength at different surfactant concentrations for the parameters fmsurf and epsurf.

surfactant concentration, fmsurf, was determined to be about 0.89 wt % (~0.045 mol %) for foam generation, as shown in Figure 5b. This indicates that when the surfactant concentration is less than 0.89 wt %, the foam strength is dependent of the surfactant concentration.

*3.1.5. Shearing Thinning-Dependent Function Parameters.* The shear-thinning flow properties of the foam are well known. The apparent viscosity of the foam typically decreases with the increasing superficial velocity, and the shear-thinning rate depends on the surfactant. In the STARS foam model, epcap describes the foam rheology. When the epcap equals to 0, the foam behaves like a Newtonian fluid, whereby the apparent viscosity does not change with the superficial velocity. For our TTM $CO_2$ foam, the value of epcap was found to be 0.68, which illustrates that TTM $CO_2$ foam is non-Newtonian. As shown in Figure 6, TTM $CO_2$ foam is shear thinning within

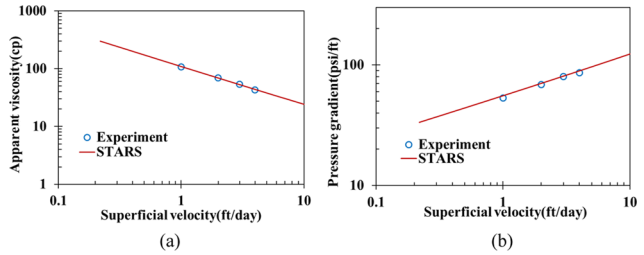


**Figure 6.** Effect of shear rates on the foam steady-state (a) apparent viscosity and (b) pressure gradient value and the STARS model fit on fmcap and epcap ($k$ = 321 mD, fg = 0.8, 120 °C, 3400 psi, 1.0 wt % TTM).

the range of total flow rates from 1 to 4 ft/day. The STARS foam parameters obtained from the above-mentioned experiments are summarized in Table 1.

**3.2. $CO_2$ Foam Flooding in the Presence of SMY Crude Oil.** *3.2.1. $CO_2$ Foam EOR.* The TTM $CO_2$ foam has demonstrated good in situ foam generation in limestone cores. This section probes $CO_2$ foam EOR and mobility control in the presence of crude oil. The experiments were performed using a two-phase (SMY crude oil and 22% TDS brine)-saturated Indiana limestone core, as previously described. As shown by a representative experiment in Figure 7, a brine flood

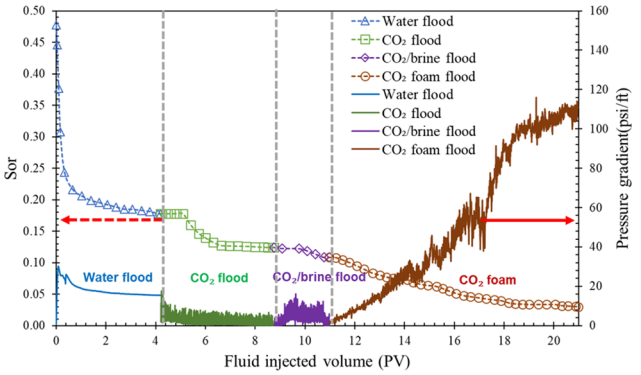


**Figure 7.** Residual oil saturation and pressure gradient for water, $CO_2$, $CO_2$–brine, and $CO_2$ foam flooding in an Indiana limestone core ($k$ = 413 mD, 4 ft/day, fg = 0.8, 1 wt % TTM, 120 °C, 3400 psi, $L \times D$ = 6 × 1.5 in.).

at 4 ft/day (labeled water flood) was conducted to achieve the two-phase saturation of brine and residual oil in the core. Afterward, the pressure and temperature of the system were increased to 3400 psi and 120 °C to initiate $CO_2$ flooding for about 4 PVs (labeled $CO_2$ flood). Co-injection of $CO_2$ gas and brine was then started at 4 ft/day with a gas fraction flow at 80% (labeled $CO_2$-brine). $CO_2$ foam commenced at around 10 PV when the pressure gradient begins to rise (labeled $CO_2$ foam), and flooding continues until the foam reached a steady-state apparent viscosity.

The oil saturation and pressure gradient for the limestone core were measured after various flooding strategies, as shown in Figure 7. The oil saturation was recorded based on the produced liquid and mass balance calculation. The oil saturation before water flood was 47.8%. After the water flood, the oil saturation was decreased to 17.8%. $CO_2$ flood decreases the oil saturation to 12.4%, and $CO_2$/brine flood decreases the oil saturation to 10.8%. $CO_2$ foam flood decreases the oil saturation to 3.0%. It takes about 10 PV of the foam injection to reach the steady state. For the $CO_2$ foam flooding, it was found that the pressure gradient increased with continuous oil production. This phenomenon may be due to the detrimental effect of oil on the foam strength. In the presence of crude oil, the $CO_2$ foam strength is significantly

**Table 1. TTM $CO_2$ Foam Parameters in Indiana Limestone Core Based on the STARS Model**

| $k$ (mD) | fmmob | fmdry | epdry | fmsurf | epsurf | fmcap | epcap |
|---|---|---|---|---|---|---|---|
| 54 | 140 | 0.383 | 116 | N/A | N/A | N/A | N/A |
| 321 | 188 | 0.238 | 70 | 0.00045 | 0.196 | $1.17 \times 10^{-6}$ | 0.68 |



DOI: 10.1021/acs.energyfuels.9b00667
Energy Fuels 2019, 33, 6038−6047

reduced and is only able to reach a stable value when the oil saturation in the core is sufficiently low. In the experiment shown in Figure 7, the limiting oil saturation for the foam to reach a steady state is around 3%.

After the foam flooding experiment is finished, the core is then flushed with 22% TDS brine until there was no longer any gas production, which is typically more than 50 PV. The surfactant concentration in the produced water was monitored. It was assumed that the surfactant is sufficiently flushed out of the core when the produced fluid is unable to foam when mechanically agitated. Afterward, a similar $CO_2$ foam flooding process was conducted in the same core but with a lower residual oil concentration of 3%. Briefly, $CO_2$ and brine co-injection at 4 ft/day and 80% gas fractional flow was conducted for about 2 PV. Then, $CO_2$ foam flooding was conducted again with 4 ft/day at 80% gas fractional flow, and the pressure data and corresponding apparent viscosity calculated based on Darcy's law are shown in Figure 8. The orange curve is also

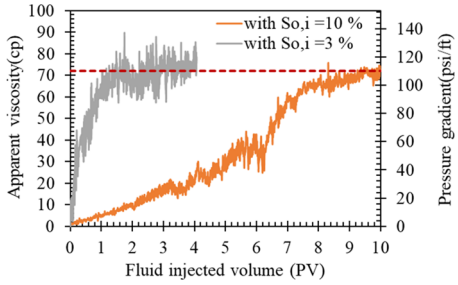


**Figure 8.** $CO_2$ foam apparent viscosity at an initial crude oil saturation of 3% (gray) and 10% (orange) in an Indiana limestone core ($k$ = 413 mD, 4 ft/day, fg = 0.8, 1 wt % TTM, 120 °C, 3400 psi, $L \times D$ = 6 × 1.5 in.).

plotted using the same data from Figure 7 during the $CO_2$ foam EOR process. These two $CO_2$ foam flooding processes, as shown in Figure 8, were injected into the same core with either $S_{o,i}$ of 3% or 10% to evaluate the role of initial crude oil saturation ($S_{o,i}$) on foam generation. It takes more than 10 PV for the $CO_2$ foam to reach the steady state at the higher $S_{o,i}$ = 10%. In comparison, when $S_{o,i}$ = 3%, the in situ $CO_2$ foam generation occurred immediately and reached steady state after 1.5 PV. The apparent viscosity of the two foam flooding processes ultimately reaches the same value. The differences of the foam generation in the two cases illustrate that the higher initial oil saturation with the SMY crude oil has a detrimental effect on the $CO_2$ foam generation using TTM surfactant under the tested conditions.

*3.2.2. Effect of Residual Oil Saturation on $CO_2$ Foam.* The quality scan experiment in the presence of 3% crude oil was conducted after the foam in situ generation experiments. The foam apparent viscosity (30−90% foam quality) with $S_{o,i}$ = 3% is higher than in the absence of oil, as shown in Figure 9. At this residual oil saturation, the oil does not have a detrimental effect on the foam strength. Thus, the apparent viscosity change of the foam was a result of the relative permeability change. In the presence of crude oil in the core, the relative permeability of the gas and brine phase decreases, which results in an increased foam apparent viscosity.

*3.2.3. Effect of Oil Fractional Flow on Foam Strength.* Based on the fractional flow theory, oil saturation could be increased by increasing the fractional flow of oil. To investigate the oil saturation effect on the foam strength, a fractional flow

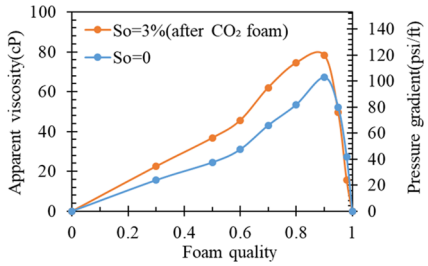


**Figure 9.** $CO_2$ foam quality with 1 wt % TTM scan without oil and with 3% crude oil present in an Indiana limestone core ($k$ = 413 mD, 4 ft/day, fg = 0.8, 1 wt % TTM, 120 °C, 3400 psi, $L \times D$ = 6 × 1.5 in.).

experiment was designed by fixing the total flow rate of the fluid (oil/gas/surfactant solution) at 4 ft/day at a constant foam quality equals to 50 or 80%. The flow rate of the oil phase[41] was changing from 0 to 20%. It was observed that when the oil fractional flow increases to 5−10%, the strength of the foam decreases sharply, as shown in Figure 10. Even

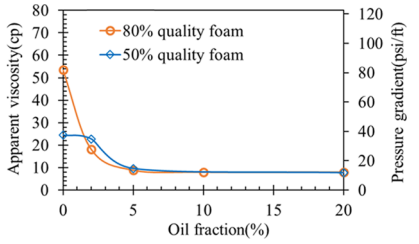


**Figure 10.** Foam flooding (1% TTM) in the presence of fractional flow of oil in an Indiana limestone core ($k$ = 413 mD, 4 ft/day, fg = 0.5 or 0.8, 1 wt % TTM, 120 °C, 3400 psi, $L \times D$ = 6 × 1.5 in.).

when the oil fractional flow is 2%, the apparent viscosity of the foam decreases from 52 to 18 cP at a foam quality of 80% and decreases from 24.5 to 23 cP when the foam quality is 50%. When the fractional flow of oil increases to higher than 5%, the apparent viscosity of the foam continues to decrease and reaches a plateau value around 8 cP for both cases.

The test results indicate that at ∼3400 psi, the $CO_2$ is miscible or near miscible with the SMY crude oil, which allows the $CO_2$ to be injected into a hydrocarbon-enriched gas phase. Under these conditions, even a very low content of the SMY crude oil can cause a sharp decrease of the foam apparent viscosity. This phenomenon of $CO_2$ foam was also observed in a sand-pack system[42] where a low fractional flow of oil could cause a significant decrease of the foam apparent viscosity under miscible conditions. In general, the TTM $CO_2$ foam experiments conducted in this manuscript can behave differently if the type of crude oil is changed. Numerically, the oil detrimental effect can be described by the oil saturation-dependent function, as shown in eq 7. To understand how these parameters affect the TTM $CO_2$ foam under reservoir conditions, a foam simulation was conducted in the next section.

**3.3. Foam Simulation in the Presence of Crude Oil.**

*3.3.1. Oil-Dependent Function in the STARS Model.* In the following simulations, the effect of fmoil and epoil parameters on TTM $CO_2$ foam behavior is discussed. By varying the values of fmoil and epoil, we can evaluate the responses of TTM $CO_2$ to different oils. The performance of the TTM $CO_2$ foam mobility control will also be discussed under these



DOI: 10.1021/acs.energyfuels.9b00667
Energy Fuels 2019, 33, 6038−6047

conditions. As previously described, the fmoil describes the critical oil saturation when the foam completely decays in the porous media, and the epoil parameter shows the sharpness of the foam decay as a function of oil saturation. A larger fmoil means that the foam can exist under high oil saturations, and a lower value of epoil means that the foam strength decays slowly when oil saturation increases. The effects of fmoil and epoil on the oil saturation dependence function are shown in Figure 11.

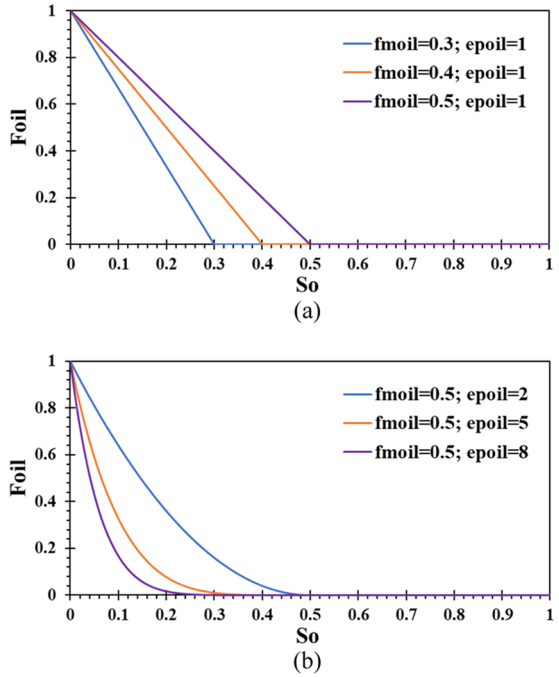


**Figure 11.** Effect of fmoil and epoil on the oil saturation dependence function.

*3.3.2. Foam Simulation in the Presence of Oil Based on TTM Foam Model Parameters.* The first foam simulation process was conducted with fmoil = 0.5, epoil = 1, and the other model parameters estimated using a 1 wt % TTM $CO_2$ foam experiment (dry-out, shear thinning, and surfactant concentration-dependent functions). The fmoil and epoil values used correspond to the case of when TTM $CO_2$ foam has a limiting oil saturation equals to 0.5, and the foam decays linearly with an increased oil saturation. The foam parameters for the simulation are shown in Table 2.

A heterogeneous model reservoir based on the permeability studied experimentally was used in the foam simulation process, as shown in Figure 12. The length of the reservoir is 500 ft with a depth of 44 ft. The simulation was performed

**Table 2. STARS Foam Parameters Used in the Reservoir Simulation**

| parameters | value |
|---|---|
| fmmob | 188 |
| fmdry | 0.238 |
| epdry | 70 |
| fmsurf | 0.00045 |
| epsurf | 0.195 |
| fmcap | $1.17 \times 10^{-6}$ |
| epcap | 0.68 |
| fmoil | 0.5 |
| epoil | 1 |

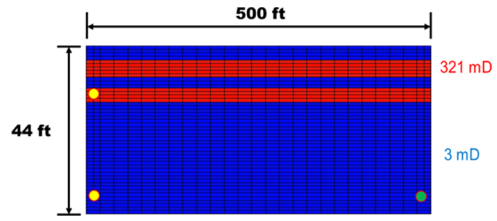


**Figure 12.** Model heterogeneous reservoir used for the simulation of $CO_2$ foam flooding process.

using a pressure 3400 psi and temperature equals to 120 °C. The model reservoir was characterized by high permeability intervals in the upper layers with the permeability of 321 mD. The lower part of the reservoir was characterized by a low permeability of 3 mD. The $CO_2$ was injected in the lower layer, and $CO_2$/brine or $CO_2$/surfactant was injected in the upper layer, as shown for the dots on the left side, and oil was produced in the production well in the bottom layer, as shown by the dot on the lower right side in Figure 12.

In the absence of the foam, fmmob was set to zero, which results in an FM equal to 1. Thus, there is no foam contribution to the flooding in this case. The reservoir was set with two horizontal injectors; one placed at the upper high permeability zone and the other was placed in the lower permeability layer. The top injector is for 80% quality $CO_2$/brine (with or without the surfactant) flooding. The other bottom injector is for only $CO_2$ flooding. The results of the oil saturation, gas saturation at different time scales are shown from Figure 13a–d.

It was found that in the absence of the foam, $CO_2$ will break through the reservoir much faster in the top high permeability zone, as shown in Figure 13a. In the presence of the foam, when the saturation of oil in the top layer is reduced, the mobility of $CO_2$ is significantly reduced, resulting in a significant increase of swept oil in the bottom zone of low permeability, as shown in Figure 13b.

The saturation of $CO_2$ profile with and without foam is shown in Figure 13c,d. When no surfactant was present, as shown in Figure 13c, the $CO_2$ breakthrough and the $CO_2$ saturation among the top-high permeability layers increase. For the case with the foam stabilized by TTM, as shown in Figure 13d, the $CO_2$ saturation in the low permeability layers on the bottom part has increased significantly due to the reduced mobility of $CO_2$ in the top layers.

The overall results are, shown in Figure 13a–d, indicating that the mobility of the $CO_2$ could be significantly reduced by generating $CO_2$ foam with TTM that helps to increase oil production while increasing $CO_2$ phase trapping in the low permeability zone.

*3.3.3. Effect of fmoil on Oil Saturation after Foam Flooding.* In this case, the same STARS foam parameters for TTM foam, as shown in Table 2, were used for the foam simulation. However, the epoil was set to 1 with changing the value of fmoil. The fmoil is for limiting oil saturation where the foam completely decays.

The motivation for this simulation is to evaluate the TTM $CO_2$ foam mobility control for various crude oils, with different values of fmoil. A higher value of fmoil indicates that the TTM foam is not sensitive to the crude oil, whereas a lower value of



DOI: 10.1021/acs.energyfuels.9b00667
Energy Fuels 2019, 33, 6038−6047

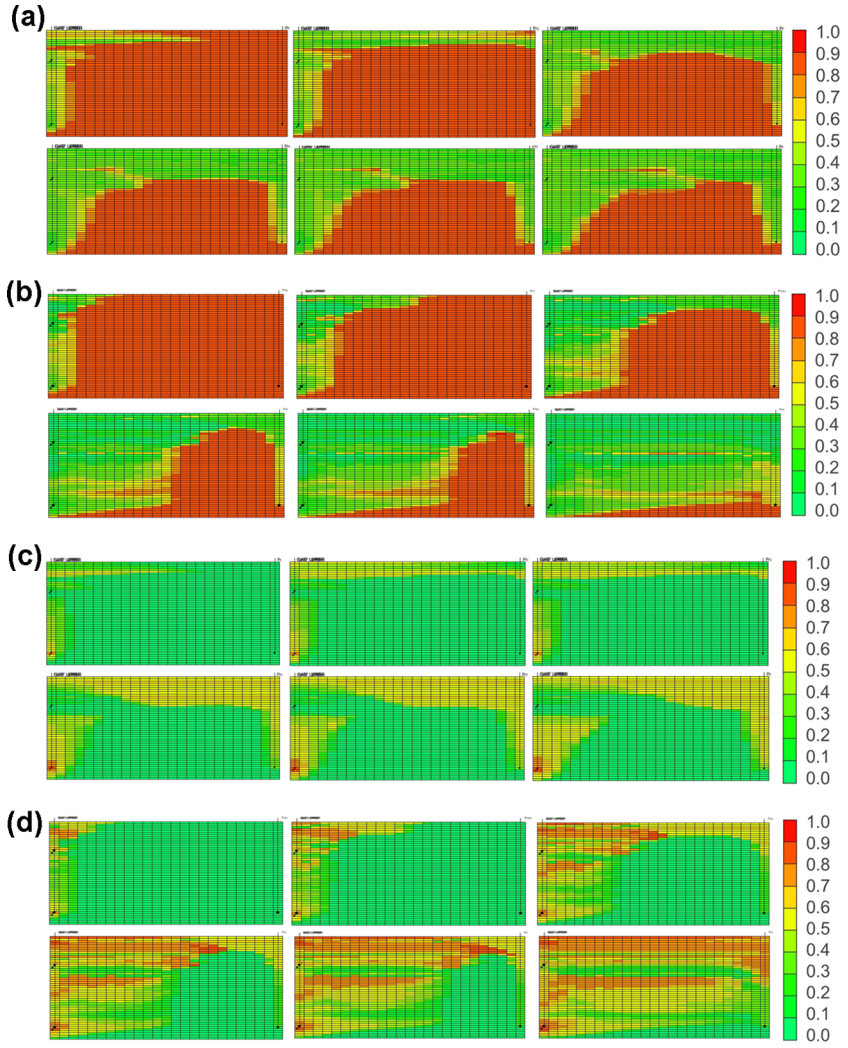


**Figure 13.** (a) Saturation of oil at 1, 2, 5, 8, 10, and 15 years with co-injection of brine and $CO_2$ (80% quality). (b) Saturation of oil at 1, 2, 5, 8, 10, and 15 years with co-injection of TTM and $CO_2$ (80% quality). (c) Saturation of $CO_2$ at 1, 2, 5, 8, 10, and 15 years with co-injection of brine and $CO_2$ (80% quality). (d) Saturation of $CO_2$ at 1, 2, 5, 8, 10, and 15 years with co-injection of TTM and $CO_2$ (80% quality).

fmoil means that the TTM foam is sensitive to the crude oil and decays quickly at low oil saturation conditions.

Shown in Figure 14 are the simulation results after 15 years of the foam flooding by increasing fmoil from 0.3 to 0.5 case.

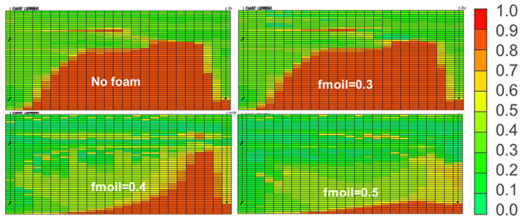


**Figure 14.** Effect of fmoil on oil saturation after 15 years of the foam flooding at a fixed epoil = 1.

In the case of fmoil = 0.3, there is an insignificant difference in the oil saturation when compared with the no foam treatment case. For the case of fmoil = 0.4, the $CO_2$ recovers a certain amount of oil from the low permeability zone due to the foam generated in situ after the oil saturation decreased less than 0.4 in the top layers. For the case of fmoil = 0.5, a significant amount of oil from the low permeability layers was recovered.

The simulation results shown in Figure 14 indicate that for TTM $CO_2$ foam under reservoir conditions, the mobility control performance is better for higher fmoil. However, if the oil is detrimental to the foam, the fmoil value will be low. Thus, the mobility control performance will be poor.

*3.3.4. Effect of epoil on Oil Saturation after Foam Flooding.* The STARS foam parameters for TTM foam shown in Table 2 are used again for the foam simulation, but now the fmoil parameter was set to 0.5 with changing the value of epoil. The epoil represents the sharpness in how the foam decays. As in the previous case, the TTM $CO_2$ foam may have different responses to various crude oils, which results in different values of epoil. A higher value of epoil means that the strength of TTM foam decreases faster when the crude oil saturation increases.

As shown in Figure 15, the case epoil = 8, when compared with no foam case, exhibited a little decrease in oil saturation after 15 years of the foam flooding. For the case of epoil = 5, the $CO_2$ mobilizes a significant amount of oil from the low permeability layer at the bottom due to the foam generated in situ after the oil saturation has decreased. For the case epoil = 2, the stronger foam could be generated as a function of decreasing oil saturation. When epoil increases, the foam



DOI: 10.1021/acs.energyfuels.9b00667
*Energy Fuels* 2019, 33, 6038−6047

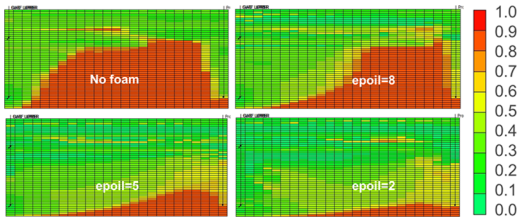


**Figure 15.** Effect of epoil on oil saturation after 15 years of the foam flooding at fixed fmoil = 0.5.

decays faster with the increasing oil saturation. These simulation results indicate that for TTM $CO_2$ foam under reservoir conditions, the mobility control performance is better for lower epoil values.

In general, for the same TTM $CO_2$ foam injected into the reservoir, the performance of mobility control significantly depends on the crude oil properties. For higher values of fmoil and lower values of epoil, the performance of TTM $CO_2$ foam is effective. This indicates that the foam−oil interactions are extremely important for determining the performance of $CO_2$ foam mobility under reservoir conditions.

## 4. CONCLUSIONS

We have demonstrated that a 1 wt % TTM surfactant can generate a strong $CO_2$ foam at 120 °C at 4 ft/day and fg = 0.8. In situ foam generation was verified in limestone core with 321 mD using co-injection and SAG injection. The STARS parameters of TTM $CO_2$ foam in limestone core were obtained by multiple variable optimization processes. The parameters fitted were dry-out, shear thinning, and surfactant concentration-dependent in corresponding functions.

TTM $CO_2$ foam could be generated in the presence of crude oil in limestone cores under reservoir conditions. The oil under miscible conditions could significantly impact the foam strength in porous media and also foam generation. A low oil saturation was found to be beneficial for TTM $CO_2$ foam to be generated more quickly under miscible conditions.

A foam simulation process in a heterogeneous reservoir was conducted using the parameters obtained from TTM $CO_2$ foam experiments. The simulation results (fmoil = 0.5, epoil = 0.1) indicate that TTM $CO_2$ foam could significantly reduce the mobility of $CO_2$ in the high permeability layer for improving swept volume in the low permeability zone and thus result in significant oil recovery. The effect of fmoil and epoil on the oil saturation profile was simulated after 15 years of $CO_2$/$CO_2$-foam injection. For a higher value of fmoil and lower value of epoil, the performance of TTM $CO_2$ foam to enhance EOR is significant.

## ■ ASSOCIATED CONTENT

### Supporting Information

The Supporting Information is available free of charge on the ACS Publications website at DOI: 10.1021/acs.energyfuels.9b00667.

Schematic details of the core flooding set-up including the pump system, core holder module, pressure transducer module, and back pressure module; diagram of the multilayer core assembly for supercritical $CO_2$ and $CO_2$ foam flooding; relative permeability curves used for STARS foam modeling; formulations and procedure of estimating the foam modeling parameters including foam dry-out function, shear thinning function, and surfactant concentration function (PDF)

## ■ AUTHOR INFORMATION

### Corresponding Authors

*E-mail: biswal@rice.edu (S.L.B.).
*E-mail: gjh@rice.edu (G.J.H.).

### ORCID

Sibani L. Biswal: 0000-0002-0610-835X

### Notes

The authors declare no competing financial interest.

## ■ ACKNOWLEDGMENTS

We acknowledge the financial support from Abu Dhabi National Oil Company (ADNOC) and the Rice University Consortium for Processes in Porous Media.

## ■ REFERENCES

(1) Enick, R. M.; Olsen, D. K.; Ammer, J. R.; Schuller, W. *Mobility and Conformance Control for CO2 EOR via Thickeners, Foams, and Gels -- A Literature Review of 40 Years of Research and Pilot Tests*; Society of Petroleum Engineers, 2012.

(2) Haugen, A.; Mani, N.; Svenningsen, S.; Brattekås, B.; Graue, A.; Ersland, G.; Fernø, M. A. Miscible and Immiscible Foam Injection for Mobility Control and EOR in Fractured Oil-Wet Carbonate Rocks. *Transp. Porous Media* **2014**, *104*, 109−131.

(3) Wang, X.; Gu, Y. Oil Recovery and Permeability Reduction of a Tight Sandstone Reservoir in Immiscible and Miscible CO2 Flooding Processes. *Ind. Eng. Chem. Res.* **2011**, *50*, 2388−2399.

(4) Cao, M.; Gu, Y. Physicochemical Characterization of Produced Oils and Gases in Immiscible and Miscible CO2 Flooding Processes. *Energy Fuels* **2013**, *27*, 440−453.

(5) Chen, S.; Li, H.; Yang, D.; Tontiwachwuthikul, P. Optimal Parametric Design for Water-Alternating-Gas (WAG) Process in a CO2-Miscible Flooding Reservoir. *J. Can. Pet. Technol.* **2010**, *49*, 75−82.

(6) Liu, Y.; Grigg, R. B.; Svec, R. K. *CO2 Foam Behavior: Influence of Temperature, Pressure, and Concentration of Surfactant*; Society of Petroleum Engineers, 2005.

(7) Zuta, J.; Fjelde, I.; Berenblyum, R. *Experimental And Simulation Of CO2-Foam Flooding In Fractured Chalk Rock At Reservoir Conditions: Effect Of Mode Of Injection On Oil Recovery*; Society of Petroleum Engineers, 2010.

(8) Skoreyko, F. A.; Villavicencio, A. P.; Rodriguez Prada, H.; Nguyen, Q. P. *Development of a New Foam EOR Model From Laboratory and Field Data of the Naturally Fractured Cantarell Field*; Society of Petroleum Engineers, 2011.

(9) Sanders, A.; Jones, R. M.; Rabie, A.; Putra, E.; Linroth, M. A.; Nguyen, Q. P. et al. *Implementation of a CO2 Foam Pilot Study in the SACROC Field: Performance Evaluation. In SPE Annual Technical Conference and Exhibition*; Society of Petroleum Engineers, 2012.

(10) Talebian, S. H.; Masoudi, R.; Tan, I. M.; Zitha, P. L. J. *Foam Assisted CO2-EOR; Concepts, Challenges and Applications*; Society of Petroleum Engineers, 2013.

(11) Patil, P. D.; Knight, T.; Katiyar, A.; Vanderwal, P.; Scherlin, J.; Rozowski, P.; Ibrahim, M.; Sridhar, G. B.; Nguyen, Q. P. *CO2 Foam Field Pilot Test in Sandstone Reservoir: Complete Analysis of Foam Pilot Response*; Society of Petroleum Engineers, 2018.

(12) Wellington, S. L.; Vinegar, H. J. *CT Studies of Surfactant-Induced CO2 Mobility Control. In SPE Annual Technical Conference and Exhibition*; Society of Petroleum Engineers, 1985.

(13) Kim, J.; Dong, Y.; Rossen, W. R. Steady-State Flow Behavior of CO2 Foam. *SPE J.* **2005**, *10*, 405−415.

(14) Mathew, E. S.; Shaik, A. R.; Al Sumaiti, A.; AlAmeri, W. Effect of Oil Presence on CO2 Foam Based Mobility Control in High



DOI: 10.1021/acs.energyfuels.9b00667
*Energy Fuels* 2019, 33, 6038−6047

Temperature High Salinity Carbonate Reservoirs. *Energy Fuels* **2018**, *32*, 2983−2992.
(15) Farzaneh, S. A.; Sohrabi, M. Experimental Investigation of CO2-Foam Stability Improvement by Alkaline in the Presence of Crude Oil. *Chem. Eng. Res. Des.* **2015**, *94*, 375−389.
(16) Alcorn, Z. P.; Fredriksen, S. B.; Sharma, M.; Rognmo, A. U.; Føyen, T. L.; Fernø, M. A.; Graue, A. *An Integrated CO2 Foam EOR Pilot Program with Combined CCUS in an Onshore Texas Heterogeneous Carbonate Field*; Society of Petroleum Engineers, 2018.
(17) Cui, L.; Ma, K.; Puerto, M.; Abdala, A. A.; Tanakov, I.; Lu, L. J.; Chen, Y.; Elhag, A.; Johnston, K. P.; Biswal, S. L.; et al. Mobility of Ethomeen C12 and Carbon Dioxide (CO2) Foam at High Temperature/High Salinity and in Carbonate Cores. *SPE J.* **2016**, *21*, 1151−1163.
(18) Zhang, C.; Li, Z.; Li, S.; Lv, Q.; Wang, P.; Liu, J.; Liu, J. Enhancing Sodium Bis(2-Ethylhexyl) Sulfosuccinate Injectivity for CO2 Foam Formation in Low-Permeability Cores: Dissolving in CO2 with Ethanol. *Energy Fuels* **2018**, *32*, 5846−5856.
(19) Wang, J.; Liang, M.; Tian, Q.; Feng, Y.; Yin, H.; Lu, G. CO2-Switchable Foams Stabilized by a Long-Chain Viscoelastic Surfactant. *J. Colloid Interface Sci.* **2018**, *523*, 65−74.
(20) Da, C.; Alzobaidi, S.; Jian, G.; Zhang, L.; Biswal, S. L.; Hirasaki, G. J.; Johnston, K. P. Carbon Dioxide/Water Foams Stabilized with a Zwitterionic Surfactant at Temperatures up to 150 °C in High Salinity Brine. *J. Pet. Sci. Eng.* **2018**, 880−890.
(21) Jian, G.; Puerto, M. C.; Wehowsky, A.; Dong, P.; Johnston, K. P.; Hirasaki, G. J.; Biswal, S. L. Static Adsorption of an Ethoxylated Nonionic Surfactant on Carbonate Minerals. *Langmuir* **2016**, *32*, 10244−10252.
(22) Abbas, S.; Sanders, A. W.; Chakraborty, D. Use of Carbon Dioxide Soluble Nonionic Surfactants for Enhanced Crude Oil Recovery. U.S. Patent US9850421B2, December 26, 2017.
(23) Jian, G.; Puerto, M.; Wehowsky, A.; Miller, C.; Hirasaki, G. J.; Biswal, S. L. Characterizing Adsorption of Associating Surfactants on Carbonates Surfaces. *J. Colloid Interface Sci.* **2018**, *513*, 684−692.
(24) Chen, Y.; Elhag, A. S.; Worthen, A. J.; Reddy, P. P.; Ou, A. M.; Hirasaki, G. J.; Nguyen, Q. P.; Biswal, S. L.; Johnston, K. P. High Temperature CO2-in-Water Foams Stabilized with Cationic Quaternary Ammonium Surfactants. *J. Chem. Eng. Data* **2016**, *61*, 2761−2770.
(25) Chen, Y.; Elhag, A. S.; Cui, L.; Worthen, A. J.; Reddy, P. P.; Noguera, J. A.; Ou, A. M.; Ma, K.; Puerto, M.; Hirasaki, G. J.; et al. CO2-in-Water Foam at Elevated Temperature and Salinity Stabilized with a Nonionic Surfactant with a High Degree of Ethoxylation. *Ind. Eng. Chem. Res.* **2015**, *54*, 4252−4263.
(26) AlSumaiti, A. M.; Hashmet, M. R.; AlAmeri, W. S.; Anto-Darkwah, E. Laboratory Study of CO2 Foam Flooding in High Temperature, High Salinity Carbonate Reservoirs Using Co-Injection Technique. *Energy Fuels* **2018**, *32*, 1416−1422.
(27) Farajzadeh, R.; Lotfollahi, M.; Eftekhari, A. A.; Rossen, W. R.; Hirasaki, G. J. H. Effect of Permeability on Implicit-Texture Foam Model Parameters and the Limiting Capillary Pressure. *Energy Fuels* **2015**, *29*, 3011−3018.
(28) Rossen, W.; Boeije, C. S. Fitting Foam-Simulation-Model Parameters to Data: II. Surfactant-Alternating-Gas Foam Applications. *SPE Reservoir Eval. Eng.* **2015**, *18*, 273−283.
(29) Boeije, C. S.; Rossen, W. R. *Gas Injection Rate Needed for SAG Foam Processes to Overcome Gravity Override*; Society of Petroleum Engineers, 2013.
(30) Da, C.; Jian, G.; Alzobaidi, S.; Yang, J. H.; Biswal, S. L.; Hirasaki, G. J.; Johnston, K. P. Design of CO2-in-Water Foam Stabilized With Switchable Amine Surfactants at High Temperature in High Salinity Brine and Effect of Oil. *Energy Fuels* **2018**, 12259.
(31) Da, C.; Elhag, A.; Jian, G.; Zhang, L.; Alzobaidi, S.; Zhang, X.; Al Sumaiti, A.; Biswal, S.; Hirasaki, G.; Johnston, K. *CO2/Water Foams Stabilized with Cationic or Zwitterionic Surfactants at Temperatures up to 120 °C in High Salinity Brine. In SPE Annual Technical Conference and Exhibition*; Society of Petroleum Engineers, 2018.
(32) Farajzadeh, R.; Lotfollahi, M.; Eftekhari, A. A.; Rossen, W. R.; Hirasaki, G. J. H. Effect of Permeability on Implicit-Texture Foam Model Parameters and the Limiting Capillary Pressure. *Energy Fuels* **2015**, *29*, 3011−3018.
(33) Zeng, Y.; Ma, K.; Farajzadeh, R.; Puerto, M.; Biswal, S. L.; Hirasaki, G. J. Effect of Surfactant Partitioning Between Gaseous Phase and Aqueous Phase on CO2 Foam Transport for Enhanced Oil Recovery. *Transp. Porous Media* **2016**, *114*, 777−793.
(34) Song, J.; Rezaee, S.; Zhang, L.; Zhang, Z.; Puerto, M.; Wani, O. B.; Vargas, F.; Alhassan, S.; Biswal, S. L.; Hirasaki, G. J. Characterizing the Influence of Organic Carboxylic Acids and Inorganic Silica Impurities on the Surface Charge of Natural Carbonates Using an Extended Surface Complexation Model. *Energy Fuels* **2019**, *33*, 957−967.
(35) Yang, S.-Y.; Hirasaki, G. J.; Basu, S.; Vaidya, R. Mechanisms for Contact Angle Hysteresis and Advancing Contact Angles. *J. Pet. Sci. Eng.* **1999**, *24*, 63−73.
(36) Ma, K.; Lopez-Salinas, J. L.; Puerto, M. C.; Miller, C. A.; Biswal, S. L.; Hirasaki, G. J. Estimation of Parameters for the Simulation of Foam Flow through Porous Media. Part 1: The Dry-Out Effect. *Energy Fuels* **2013**, *27*, 2363−2375.
(37) Zeng, Y.; Muthuswamy, A.; Ma, K.; Wang, L.; Farajzadeh, R.; Puerto, M.; Vincent-Bonnieu, S.; Eftekhari, A. A.; Wang, Y.; Da, C.; et al. Insights on Foam Transport from a Texture-Implicit Local-Equilibrium Model with an Improved Parameter Estimation Algorithm. *Ind. Eng. Chem. Res.* **2016**, *55*, 7819−7829.
(38) Kapetas, L.; Vincent Bonnieu, S.; Farajzadeh, R.; Eftekhari, A. A.; Shafian, S. R. M.; Bahrim, R. Z. K.; Rossen, W. R. Effect of Permeability on Foam-Model Parameters: An Integrated Approach from Core-Flood Experiments through to Foam Diversion Calculations. *Colloids Surf., A* **2017**, *530*, 172−180.
(39) Farajzadeh, R.; Lotfollahi, M.; Eftekhari, A. A.; Rossen, W. R.; Hirasaki, G. J. H. Effect of Permeability on Implicit-Texture Foam Model Parameters and the Limiting Capillary Pressure. *Energy Fuels* **2015**, *29*, 3011−3018.
(40) Jones, S. A.; Laskaris, G.; Vincent-Bonnieu, S.; Farajzadeh, R.; Rossen, W. R. Effect of Surfactant Concentration on Foam: From Coreflood Experiments to Implicit-Texture Foam-Model Parameters. *J. Ind. Eng. Chem.* **2016**, *37*, 268−276.
(41) Amirmoshiri, M.; Zeng, Y.; Chen, Z.; Singer, P. M.; Puerto, M. C.; Grier, H.; Bahrim, R. Z. K.; Vincent-Bonnieu, S.; Farajzadeh, R.; Biswal, S. L.; et al. Probing the Effect of Oil Type and Saturation on Foam Flow in Porous Media: Core-Flooding and Nuclear Magnetic Resonance (NMR) Imaging. *Energy Fuels* **2018**, No. 11177.
(42) Chen, H.; Elhag, A. S.; Chen, Y.; Noguera, J. A.; AlSumaiti, A. M.; Hirasaki, G. J.; Nguyen, Q. P.; Biswal, S. L.; Yang, S.; Johnston, K. P. Oil Effect on CO2 Foam Stabilized by a Switchable Amine Surfactant at High Temperature and High Salinity. *Fuel* **2018**, *227*, 247−255.


DOI: 10.1021/acs.energyfuels.9b00667
*Energy Fuels* 2019, 33, 6038−6047